

Raman lasing and other nonlinear effects based on ultrahigh-*Q* CaF_2 optical resonator

Tong Xing(邢彤), Enbo Xing(邢恩博), Tao Jia(贾涛), Jianglong Li(李江龙), Jiamin Rong(戎佳敏), Yanru Zhou(周彦汝), Wenyao Liu(刘文耀), Jun Tang(唐军), and Jun Liu(刘俊)

Citation: Chin. Phys. B, 2022, 31 (**10**): 104204. DOI: 10.1088/1674-1056/ac8728
Journal homepage: http://cpb.iphy.ac.cn; http://iopscience.iop.org/cpb

What follows is a list of articles you may be interested in

High-efficiency photon-electron coupling resonant emission in GaN-based microdisks on Si

Menghan Liu(刘梦涵), Peng Chen(陈鹏), Zili Xie(谢自力), Xiangqian Xiu(修向前), Dunjun Chen(陈敦军), Bin Liu(刘斌), Ping Han(韩平), Yi Shi(施毅), Rong Zhang(张荣), Youdou Zheng(郑有炓), Kai Cheng(程凯), Liyang Zhang(张丽阳)

Chin. Phys. B, 2020, 29 (**8**): 084203. DOI: 10.1088/1674-1056/ab9443

Silica-based microcavity fabricated by wet etching

H Long(龙浩), W Yang(杨文), L Y Ying(应磊莹), B P Zhang(张保平)

Chin. Phys. B, 2017, 26 (**5**): 054211. DOI: 10.1088/1674-1056/26/5/054211

Wavelength tunable ultra-short pulses based on a flat broadbandspectrum generated in a nonlinear ytterbium-dopedfiber amplifier

Run-Qin Xu(徐润亲), Zi-Kai Dong(董自凯), Jin-Rong Tian(田金荣), Ke-Xuan Li(李克轩), Yan-Rong Song(宋晏蓉)

Chin. Phys. B, 2017, 26 (**1**): 014207. DOI: 10.1088/1674-1056/26/1/014207

Superscattering-enhanced narrow band forward scattering antenna

Hu De-Jiao, Zhang Zhi-You, Du Jing-Lei

Chin. Phys. B, 2015, 24 (**10**): 104202. DOI: 10.1088/1674-1056/24/10/104202

Low threshold fiber taper coupled rare earth ion-doped chalcogenide microsphere laser

Li Chao-Ran, Dai Shi-Xun, Zhang Qin-Yuan, Shen Xiang, Wang Xun-Si, Zhang Pei-Qing, Lu Lai-Wei, Wu Yue-Hao, Lv She-Qin

Chin. Phys. B, 2015, 24 (**4**): 044208. DOI: 10.1088/1674-1056/24/4/044208

Raman lasing and other nonlinear effects based on ultrahigh-Q CaF_2 optical resonator

Tong Xing(邢彤), Enbo Xing(邢恩博)†, Tao Jia(贾涛), Jianglong Li(李江龙), Jiamin Rong(戎佳敏), Yanru Zhou(周彦汝), Wenyao Liu(刘文耀), Jun Tang(唐军)‡, and Jun Liu(刘俊)

Key Laboratory of Electronic Testing Technology, School of Instrument and Electronics, North University of China, Taiyuan 030051, *China*

(Received 10 May 2022; revised manuscript received 18 July 2022; accepted manuscript online 5 August 2022)

The calcium fluoride (CaF_2) whispering gallery mode crystalline resonator is an excellent platform for nonlinear optical applications because of the decreasing in threshold caused by ultrahigh quality (Q) factor. In this paper, we achieved the observation of Raman lasing, first-order Raman comb, and second-order Raman lasing in a CaF_2 disk resonator with a diameter of 4.96 mm and an ultrahigh-Q of 8.43×10^8 at 1550-nm wavelength. We also observed thermal effects in CaF_2 disk resonator, and the threshold of thermo-optical oscillation is approximately coincident with Raman lasing, since the intracavity power increases rapidly when the power reaches the threshold, and higher input pump power results in longer thermal drift and higher Raman emission power. With a further increase in pump power, the optical frequency combs range is from 1520 nm to 1650 nm, with a wavelength interval of 4×FSR. It is a promising candidate for optical communication, biological environment monitoring, spectral analysis, and microwave signal sources.

Keywords: whispering gallery mode, crystalline resonator, Raman lasing, nonlinear effects, thermo-optical oscillation, optical frequency combs

PACS: 42.55.Ye, 42.60.Da, 42.65.–k **DOI:** 10.1088/1674-1056/ac8728

1. Introduction

Achieving efficient nonlinear optical interactions at low optical power has always been one of the main goals of nonlinear optics.[1–5] Various nonlinear optical effects, such as frequency doubling,[6] frequency mixing,[7] Raman scattering,[8,9] Brillouin scattering,[10] and other effects[11] have broad prospects in optical computing, quantum information processing, precision spectroscopy, optical communication, biological imaging, and many other fields.[12,13] The whispering gallery mode (WGM) resonators are fabricated with a variety of materials including silicon, sapphire, fused silica, fluoride crystalline, lithium ninobate, and other optical glasses. Owing to their ultrahigh quality (Q) factor and small mode volume, optical resonators significantly enhance light-matter interactions and establish extremely high circulating intracavity intensities, thereby reducing the pump threshold for nonlinear processes. The frequency conversion of the pump light can also be achieved at low power, so the optical resonator becomes an ideal platform to study various nonlinear effects.[14–16]

Recently, fluoride crystals, such as calcium fluoride (CaF_2), magnesium fluoride (MgF_2),[17] barium fluoride (BaF_2),[18] and strontium fluoride (SrF_2)[19] have been equally demonstrated to have ultrahigh Q in the near-IR, such an ultrahigh Q attracts extremely great attention in various research fields.[20–22] Another advantage of crystalline materials for the fabrication of the resonators is that they can be stable against humidity, and do not degrade Q when exposed to atmospheric water vapor. A CaF_2 resonator with $Q > 10^{11}$ at 1550 nm has been fabricated and reported.[23] Such an ultrahigh Q greatly reduces the excitation threshold of nonlinear effects in the resonator, and it is easy to obtain laser emission based on nonlinear effects even in materials without significant nonlinearity.[24–26] Therefore, the CaF_2 resonator with ultrahigh Q, small mode volume, high stability, and low noise interference has become the best choice for nonlinear optical applications.[27,28]

Here, we theoretically analyze the Raman threshold of the CaF_2 resonator, and obtain the relationship between Q, mode volume (V_m) of the resonator, and the Raman threshold. Meanwhile, we experimentally demonstrate Raman lasing, first-order Raman comb, and the second-order Raman lasing in a millimeter size CaF_2 WGM disk resonator with ultrahigh-Q factor of 8.43×10^8 at 1550 nm. We also report the observation and characterization of thermal effects due to the negative thermo-optic coefficient and the positive thermo-expansion coefficient. At the same time, the threshold for thermo-optical oscillation is approximately coincident with Raman lasing. With a further increase in pump power, the optical frequency combs range is from 1520 nm to 1650 nm, with a wavelength interval of $4\times$FSR. And the adjustment of the optical frequency combs can be realized by using the frequency tuning of the pump light, which have great applications in optical communication, biological environment monitoring,

†Corresponding author. E-mail: xiaoxing1228@126.com
‡Corresponding author. E-mail: tangjun@nuc.edu.cn

© 2022 Chinese Physical Society and IOP Publishing Ltd

spectral analysis, and microwave signal sources.

2. Theoretical analysis and discussion

For the first-order Raman lasing output in the optical resonator, the coupled mode equation is established, which is expressed as

$$\frac{\mathrm{d}E_\mathrm{p}}{\mathrm{d}z} = -\frac{1}{2}\frac{\omega_\mathrm{p}}{\omega_\mathrm{R}}\frac{c}{n_\mathrm{eff}} g_\mathrm{R} E_\mathrm{R}^2 E_\mathrm{p}, \tag{1}$$

$$\frac{\mathrm{d}E_\mathrm{R}}{\mathrm{d}z} = \frac{1}{2}\frac{c}{n_\mathrm{eff}} g_\mathrm{R} E_\mathrm{R}^2 E_\mathrm{R}, \tag{2}$$

where E_p and E_R are the pump light energy and stimulated Raman laser energy, respectively, c is the speed of light, n_eff is the effective refractive index of the resonator, ω_p and ω_R are the pump light frequency and the stimulated Raman laser frequency, respectively, and $g_\mathrm{R} = 2.4\times10^{-13}$ m/W[22] is the Raman gain coefficient of the CaF_2 resonator.

The mode volume (V_m) of the CaF_2 resonator is defined as the ratio of the full-space integral of the mode field energy density to the maximum energy density, and is expressed as

$$V_\mathrm{m} = \frac{\int n^2(\boldsymbol{r})\,|\boldsymbol{E}(\boldsymbol{r})|^2\,\mathrm{d}^3\boldsymbol{r}}{\max(n^2(\boldsymbol{r})\,|\boldsymbol{E}(\boldsymbol{r})|^2)}, \tag{3}$$

where $\boldsymbol{E}(\boldsymbol{r})$ is the electric field vector, $n^2(\boldsymbol{r})\,|\boldsymbol{E}(\boldsymbol{r})|^2$ is the energy density at a point in the resonator. The V_m affects the energy density of the WGM in the resonator. A smaller mode volume corresponds to a larger energy density, which enhances the interaction between light and matter and is beneficial to lowering the threshold of nonlinear effects.

The basis of Raman laser is stimulated Raman scattering which is a process of obtaining Raman gain in materials through nonlinear effects. In the process of stimulated Raman scattering, photons with red-shifted and blue-shifted frequencies are generated. The lasing threshold occurs when cavity round-trip gain equals round-trip loss. For an intensity-dependent gain coefficient, the minimum Raman threshold can be simplified as[21]

$$P_\mathrm{th}^\mathrm{min} = \frac{\pi^2 n^2}{\lambda_\mathrm{p}\lambda_\mathrm{R}}\frac{V_\mathrm{m}}{g_\mathrm{R}}\frac{1}{Q_\mathrm{R}Q_\mathrm{p}}, \tag{4}$$

where λ_p and λ_R are the pump light wavelength and the stimulated Raman laser wavelength, respectively, $n = 1.426$ is the refractive index of the CaF_2 resonator, Q_P and Q_R are quality factors for the pump and Raman wavelengths, respectively, and V_m is the mode volume. If the Q factor is the same for pump and Raman wavelengths, the Raman threshold is proportional to the ratio V_m/Q^2. Thus, the low Raman lasing threshold and efficient cascaded operation is made possible by the ultrahigh-Q of the WGM crystalline resonator.

According to Eq. (4), the relationship between the Raman threshold and the Q and the V_m can be obtained. It can be seen from Fig. 1 that Q is inversely proportional to the Raman threshold, that is, as Q increases, the Raman threshold gradually decreases; the V_m is proportional to the Raman threshold, that is, as the mode volume decreases, the Raman threshold decreases. Therefore, choosing a ultrahigh-Q, small mode volume CaF_2 resonator can further reduce the Raman threshold.

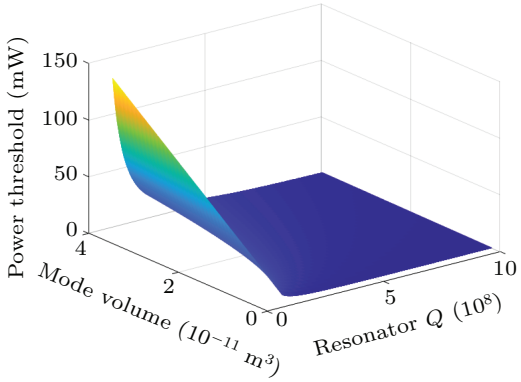


Fig. 1. Relationship between mode volume and Q of CaF_2 resonator and power threshold for Raman laser generation.

3. Experimental results and discussion

3.1. Experimental setup and characterization

The experimental setup shown in Fig. 2(a) is used to characterize the Raman lasing and other nonlinear effects based on the CaF_2 resonator system. A continuous-wave tunable laser (DLC pro) around 1550 nm with a linewidth of 10 kHz passes through the isolator and enters the CaF_2 resonator via the fiber-taper. The wavelength of the laser is scanned by signal generator (SG) to obtain the transmission spectrum for characterization of the resonator. The fiber-baser polarization controller (PC) is used to optimize the coupling strength. The light out of the fiber taper is connected with the beam splitter to the low-noise photodetector (PD) and wavelength division multiplexer (WDM) respectively. PD convert optical signals into electrical signals and then connect to oscilloscopes (OSC) for data acquisition and analysis processing. The WDM separates the pump laser and the Raman laser, and then connects them to the optical spectrum analyzer (OSA) for display. The CaF_2 crystalline WGM resonator is fabricated by single point diamond cutting and mechanical polishing method. The radius of the CaF_2 resonator is 2.48 mm, the thickness is 0.5 mm and the shape of cylinder blanks. The tapered fiber with the diameter of about 2 μm serves as the input and output ports, and the coupling to the CaF_2 resonator is accomplished by evanescent field coupling using a nano-positioning system. Figure 2(b) is the schematic diagram of fiber coupling in CaF_2 resonator. Figure 2(c) is the calculated Q factor for CaF_2 resonator of 8.43×10^8 and remains stable under normal atmospheric conditions. Once inside the clean room environment or vacuum, the Q can be preserved on a very high level for indefinite amount of time, for which our experiments are conducted in the clean room.

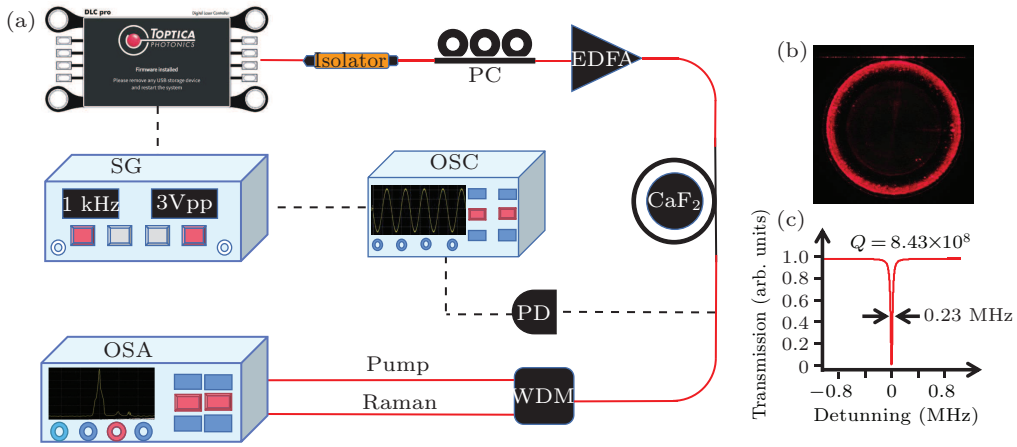


Fig. 2. (a) Diagram of the measurement setup for characterizing the nonlinear optical processes based on high-Q CaF_2 optical resonator. (b) Schematic diagram of fiber coupling in CaF_2 resonator. (c) The calculated Q for CaF_2 resonator of 8.43×10^8. DLC: pro continuous-wave tunable laser, PC: polarization controller, EDFA: erbium-doped fiber amplifier, PD: photodetector, OSC: oscilloscope, SG: signal generator, OSA: optical spectrum analyzer, WDM: wavelength division multiplexer.

3.2. Raman lasing measurement

For Raman lasing measurement, the pump wavelength is 1550.58 nm, and the pump power gradually increases from 100 μW. When the pump power is increased to 33 mW, the first-order Raman laser with the signal to noise ratio (SNR) of 46 dB is observed on the optical spectrum analyzer, as shown in Fig. 3(a). Similarly, when the pump power is gradually increased to 36 mW, the first-order Raman comb appears in Fig. 3(b) and the second-order Raman lasing appears when the pump power is increased to 45 mW in Fig. 3(c). Raman combs result from the delayed molecular response of the host medium to the laser excitation. Thanks to the low lasing threshold, the first Stokes radiation to longer wavelengths is feasible, resulting in Raman combs. By further enhancing the pump power, the intracavity first Stokes power will be sufficiently high to act as a secondary pump source to enable the second Stokes lasing at 1722.19 nm, as shown in Fig. 3(c). The transition from Fig. 3(b) to Fig. 3(c) is because the energy coupling from the side modes to the second Stokes, when the second Stokes existed. Since the side modes has lower gain than that of the central mode, so only the central mode survived.[29]

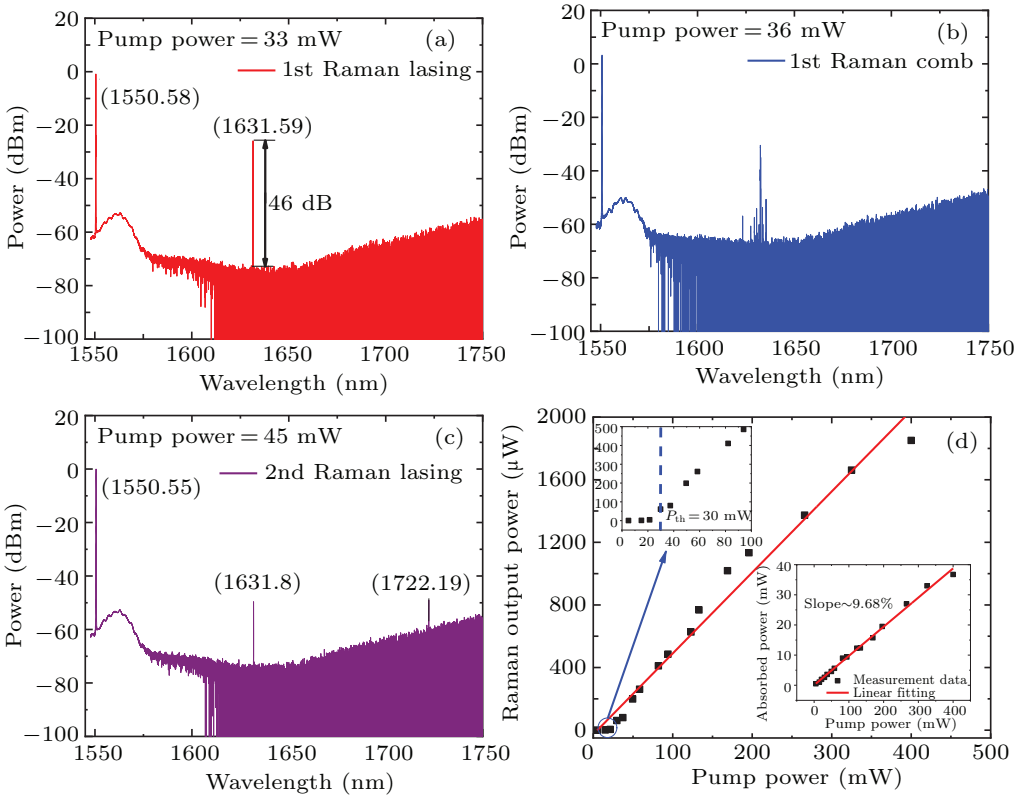


Fig. 3. Observation of cascaded Raman lasing and threshold measurement. (a) First-order Raman lasing at 1631.59 nm. (b) First-order Raman comb generation. (c) Second-order Raman lasing generation. (d) Raman output power as a function of the pump power based on a diameter of 4.96-mm resonator.

In order to measure the Raman threshold, we plot the Raman output power as a function of pump power in Fig. 3(d). The measurement shows a linear dependency and indicates the pump power threshold is 30 mW for a diameter of 4.96-mm CaF_2 resonator. We also plot the relationship between the pump power and the cavity absorbed power, as shown in the inset of Fig. 3(d). The actual power entering the resonator is only 9.68% of the pump power, the calculated conversion efficiency is about 5.27%. The power of the Raman lasing peak seems very low is because the attenuator is connected before connecting to the OSA during the experiment. The first-order Raman comb threshold pump power is 36 mW, and the second-order Raman lasing is 45 mW. The reasons for the low conversion efficiency mainly include the following aspects: (i) the detuning loss caused by the frequency scanning of the pump laser; (ii) the loss at the connection of various devices; (iii) in our experiment, we use the 'zero-gap' coupling state, that is, the tapered fiber is attached to the surface of the resonator, the influence of environmental fluctuation noise is suppressed, but reduces the Q.

Since Raman lasing threshold is proportional to V_m/Q^2, mode volume to quality factor squared ratio, it is natural to expect improvements in efficiency and threshold for a cavity with higher Q factor. The higher the Q (theoretical $Q \approx 10^{14}$) and the smaller the mode volume (V-shaped), the lower the Raman threshold (a few μW), so that the crystalline WGM resonators can become efficient and compact Raman converters. Next, we will prepare V-shaped resonator to further reduce the mode volume and thus lower the Raman threshold.

3.3. Thermal effect and Raman laser

When the input power increases above 30 mW, a strong heat accumulation occurs inside the resonator, resulting in thermal effect. The heat generated by the absorbed optical power in the mode volume elevates the temperature very rapidly. As the cavity temperature varies, n_{eff} and R change due to the thermo-optic (TO) effect ($\mathrm{d}n/\mathrm{d}T = -1.14 \times 10^{-5}\ \mathrm{K}^{-1}$) and thermal expansion (TE) effect ($\mathrm{d}R/R\mathrm{d}T = 1.87 \times 10^{-5}\ \mathrm{K}^{-1}$), respectively, giving rise to the resonance shift. While taking the direction of the wavelength shift into consideration, we scan the pump laser wavelength in the long to short wavelength direction. The scanning voltage of the laser is 1.5 V, and the scanning frequency is 10 Hz, as shown in the upper picture of Fig. 4(a). When the pump light scans into the resonant peak in the long wavelength direction, the thermal effect will push the resonant peak to move in the opposite direction due to the negative TO effect, and the compressed resonant peak will be obtained on the transmission spectrum. On the contrary, when the pump light scans to the short wavelength and enters the resonant peak, the pump light will stay in the resonant peak for a long time, and a broadened resonant peak will be obtained in the transmission spectrum, as shown in the lower picture of Fig. 4(a).

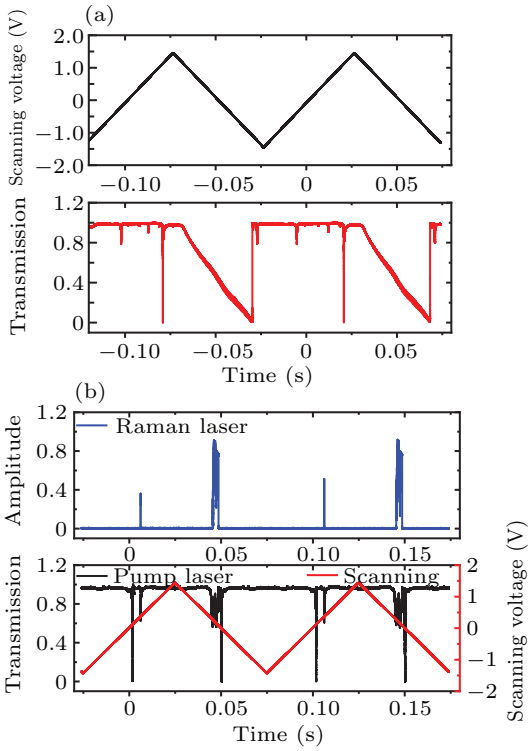


Fig. 4. (a) Thermal nonlinear effects in CaF_2 resonator. (b) The pump laser and Raman laser from the WDM on the OSC.

Figure 4(b) uses the wavelength division multiplexer (WDM) to separate the pump laser and the Raman laser, and then connect them to the oscilloscope for simultaneous observation. CaF_2 resonator has a negative TO coefficient and a positive TE coefficient, these two parameters will cause completely opposite changes in the resonance wavelength, resulting in the fluctuation of the intracavity power, so the output light field exhibits periodic oscillation, that is, thermo-optical oscillation can be generated, as shown in the lower picture of Fig. 4(b). When the power reaches the threshold, the intracavity power increases rapidly, the Raman emission power turns into laser oscillation. A higher input pump power results in a longer thermal drift and a higher Raman emission power while the threshold coupled power is maintained. However, different modes have different Q and require different pump power to generate thermal effects. When the pump power is greater than 30 mW, the mode with higher Q will first generate thermo-optic oscillation, while the mode with lower Q does not observe the phenomenon, that is, the relatively lower Q does not generate Raman laser accordingly. Furthermore, thermal broadening and thermal compression occur in pairs, located on the left and right sides of the triangular wave, respectively. In order to see the paired phenomenon more intuitively, we added triangular waves in Fig. 4(b). And in the experiment, the threshold for generating thermo-optical oscillation is also 30 mW, that is, Raman lasing is always accompanied by thermo-optical oscillations. It was found that the

threshold for the oscillations is approximately coincident with Raman lasing threshold.

3.4. Other nonlinear effects

As the pump power increases, the energy will be concentrated in the ultrahigh-Q resonator, the resonant frequency of the resonator and the detuning of the pump light will reach a balance point, and then the degenerate four-wave mixing (FWM) effect will appear. Further broadening of the FWM results in an optical frequency combs. When the power reaches the threshold, the intracavity power increases rapidly because the Kerr effect causes a rapid redshift of the resonance wavelength. The wavelength of the pump light power is set to 1550 nm, when the input power is set to 80 mW, after the energy is accumulated in the resonator, the primary comb are generated due to the FWM effect. Since the pump power energy is high enough, the energy in the resonator is further accumulated, and the secondary combs appears due to the cascaded FWM effect. The wavelength range of optical frequency comb extends from 1520 nm to 1650 nm and exceeds 120 nm, as shown in Fig. 5(a).

The pump wavelength is swept from short to long wavelengths while gradually increasing the power from 100 μW to 80 mW. When a sideband appears near the pump wavelength, stop increasing the pump power, detuning the pump wavelength from blue to the resonance peak, and observe the change of the comb teeth. At this time, several symmetrical spectrum lines appear around the pump wavelength, which are mainly composed of multiple FSRs. When the pump wavelength gradually approaches the resonance peak from blue detuning, the main combs have strong sideband effects and excite regular and gradually denser secondary combs. With the further reduction of the detuning amount of the pump wavelength, the sideband effect continues to strengthen, and more spectrum can be generated. The secondary combs next to the main comb continue to expand, the spectrum becomes denser, and finally an optical frequency comb is formed. The modulation of the optical frequency combs can be achieved by using the frequency tuning of the pump light.

The power and mode spacing of the optical frequency comb are not uniform, which is caused by the changed temperature of the resonator absorbed optical power and the existence of abundant resonance modes in the CaF_2 resonator, and the interaction between different modes. This temperature change leads to a modification of the refractive index of calcium fluoride which affects the optical path length of the resonator modes. In order to reduce the influence on the optical frequency comb, it is necessary to improve the fabrication process and continuously modify the shape to prepare a V-type crystal resonator. In addition, the mutual coupling of other nonlinear effects and the optical frequency comb effect will also produce some burrs, thus affecting the comb mode spacing. Therefore, it is necessary to precisely control the power to reduce the influence of other nonlinear effects in the experiment.

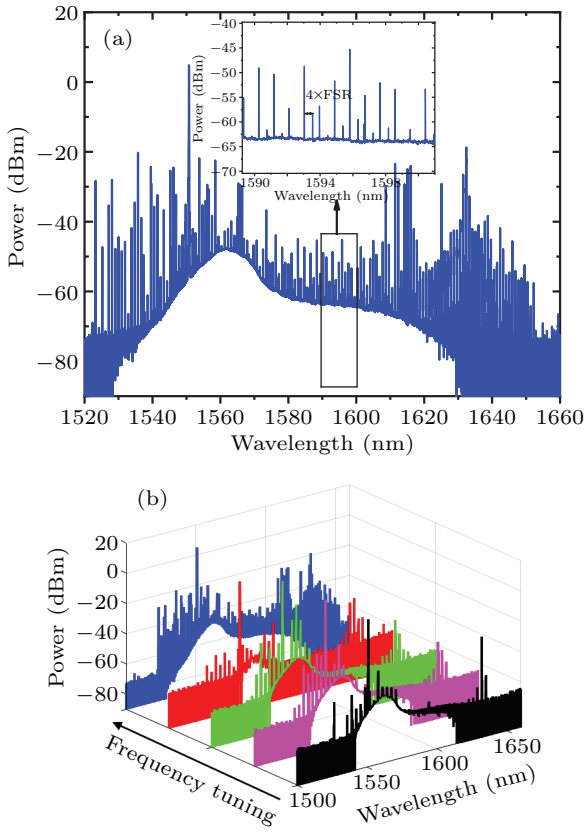


Fig. 5. (a) Optical frequency combs with wavelength range from 1520 nm to 1650 nm in CaF_2 resonator. (b) The influence of frequency tuning on optical frequency combs.

4. Conclusion

In conclusion, we theoretically analyzed the Raman threshold of the CaF_2 resonator, and obtained the Q is inversely proportional to the Raman threshold, the mode volume (V_m) of the resonator is proportional to the Raman threshold, therefore, choosing an ultrahigh Q, small mode volume CaF_2 resonator can further reduce the Raman threshold. Meanwhile, we experimentally demonstrated Raman lasing, first-order Raman comb, and the second-order Raman lasing in a CaF_2 disk resonator with a diameter of 4.96 mm and an ultrahigh Q of 8.43×10^8 at 1550-nm wavelength. At the same time, we also observed thermal effects in CaF_2 disk resonators, and obtained the threshold for thermo-optical oscillations is approximately coincident with Raman lasing. With a further increase in pump power, we observed optical frequency combs with wavelengths from 1520 nm to 1650 nm, with the range greater than 120 nm and a wavelength interval of $4\times$FSR. This work provides a comprehensive understanding of the Raman lasing and other nonlinear effects, which has great applications in optical communication, biological environment monitoring, spectral analysis, and microwave signal sources.

Acknowledgements

Project supported by the National Natural Science Foundation of China (Grant Nos. 51727808, 51922009, 52005457, and 62004179) and the Fund from the Key Laboratory of Quantum Sensing and Precision Measurement of Shanxi Province, China (Grant No. 201905D121001).

References

[1] Kippenberg T J, Spillane S M and Vahala K J 2004 *Phys. Rev. Lett.* **93** 083904
[2] Del'Haye P, Schliesser A, Arcizet O, Wilken T, Holzwarth R and Kippenberg T J 2007 *Nature* **450** 1214
[3] Herr T, Brasch V, Jost J D, Wang C Y, Kondratiev N M, Gorodetsky M L and Kippenberg T J 2014 *Nat. Photon.* **8** 145
[4] Ilchenko V S, Savchenkov A A, Matsko A B and Maleki L 2004 *Phys. Rev. Lett.* **92** 043903
[5] Xu T, Chen Y and Lin J 2017 *Chin. Phys. B.* **26** 120201
[6] Fiedler K, Schiller S, Paschotta R, Kürz P and Mlynek J 1993 *Opt. Lett.* **18** 1786
[7] Yang Q F, Yi X, Yang K Y and Vahala K 2017 *Nat. Phys.* **13** 53
[8] Grudinin I S, Matsko A B and Maleki L 2007 *Opt. Express* **15** 3390
[9] Cai X L, Zhou C H, Zhou D J, Liu J B, Guo J W and Gui L 2015 *Chin. Phys. Lett.* **32** 114207
[10] Lin G, Diallo S, Saleh K, Martinenghi R, Beugnot J C, Sylvestre T and Chembo Y K 2015 *Phys. Rev. lett.* **45** 410
[11] Wang J, Sheng A G, Huang X, Li R Y and He G Q 2020 *Chin. Phys. B.* **29** 034207
[12] Liang W, Eliyahu D, Ilchenko V S, Savchenkov A A, Matsko A B, Seidel D and Maleki L 2015 *Nat. Commun.* **6** 7957
[13] Papp S B, Beha K, Del'Haye P, Quinlan F, Lee H, Vahala K J and Diddams S A 2014 *Optica* **1** 10
[14] Lin G and Chembo Y K 2016 *Opt. Lett.* **41** 3718
[15] Griffith A G, Yu M, Okawachi Y, Cardenas J, Mohanty A, Gaeta A L and Lipson M 2016 *Opt. Express* **24** 13044
[16] Karpov M, Guo H, Kordts A, Brasch V, Pfeiffer M H P, Zervas M, Geiselmann M and Kippenberg T J 2016 *Phys. Rev. Lett.* **116** 103902
[17] Liang W, Savchenkov A A, Matsko A B, Ilchenko V S, Seidel D and Maleki L 2011 *Opt. Lett.* **36** 2290
[18] Lin G P, Diallo S, Saleh K, Martinenghi R, Beugnot J C, Sylvestre T and Chembo Y K 2014 *Appl. Phys. Lett.* **105** 231103
[19] Lecaplain C, Javerzac-Galy C, Gorodetsky M L and Kippenberg T J 2016 *Nat. Commun.* **7** 13383
[20] Grudinin I S, Ilchenko V S and Maleki L 2006 *Phys. Rev. A* **74** 063806
[21] Grudinin I S and Maleki L 2007 *Opt. Lett.* **32** 166
[22] Grudinin I S and Maleki L 2008 *J. Opt. Soc. Am. B* **25** 594
[23] Savchenkov A A, Matsko A B, Ilchenko V S and Maleki L 2007 *Opt. Express* **15** 6768
[24] Okawachi Y, Yu M, Venkataraman V, Latawiec P M, Griffith A G, Lipson M, Lončar M and Gaeta A L 2017 *Opt. Lett.* **42** 2786
[25] Matsko A B, Savchenkov A A, Liang W, Ilchenko V S, Seidel D and Maleki L 2011 *Opt. Lett.* **36** 2845
[26] Gorodetsky M L and Ilchenko V S 1999 *J. Opt. Soc. Am. B* **16** 147
[27] Wang M Y, Yang Y, Meng L, Jin X and Wang K 2019 *Chin. Opt. Lett.* **17** 111401
[28] Savchenkov A A, Liang W, Ilchenko V, Matsko A and Maleki L 2018 *IEEE J. Sel. Top. Quantum Electron.* **24** 2900111
[29] Sheng Q, Li R, Lee A J, Spence D J and Pask H M 2019 *Opt. Express* **27** 8540